치의학석사 학위논문

Effect of decompression on the bone healing of mandibular osteomyelitis in rat

백서 하악 골수염에서 감압술 효과

2021 년 2 월

서울대학교 대학원

치의과학과 구강악안면외과학 전공

Buyanbileg Sodnom-Ish

Effect of decompression on the bone healing of mandibular osteomyelitis in rat

지도교수 김 성 민

이 논문을 치의과학석사 학위논문으로 제출함

2020년 12월

서울대학교 대학원

치의과학과 구강악안면외과학 전공

Buyanbileg Sodnom-Ish

Buyanbileg Sodnom-Ish의 석사학위논문을 인준함

2020년 12월

위 원 장 이 종 호 (인)

부위원장 김 성 민 (인)

위 원 양 훈 주 (인)

Abstract

Effect of decompression on the bone healing of mandibular osteomyelitis in rat

Buyanbileg Sodnom-Ish

Program in Oral and Maxillofacial Surgery, Department of Dental Science, Graduate School, Seoul National University

(Directed by Professor Soung Min Kim)

Introduction

Osteomyelitis (OM) of the jaw is usually caused by odontogenic infection or by a variety of other reasons which result in jaw bone destruction. Microorganisms such as *Staphylococcus aureus* (*S. aureus*) are known to be significant pathogens at the pathogenesis of OM. Decompression using a drain is a reliable technique, which releases the intraluminal pressure causing reduction of cyst and allows gradual bone regeneration from the periphery. The aim of this study was to analyze the effectiveness of decompression in an OM rat mandible model.

Materials and methods

A 4 mm diameter defect was made on the mandibles of 14 male Sprague-Dawley rats (8 weeks old with weight of 230.13+/-13.87 g) and 20 μl of $1x10^7$ CFU/ml *S. aureus* was inoculated. Two weeks later, the animals were randomly divided into non-treatment control (C1), curettage only control (C2),

curettage and decompression using drain (E1), and curettage and decompression using drain with normal saline irrigation (E2) groups. After four weeks, the animals were assessed with micro-computed tomography (micro-CT), histology stained with hematoxylin and eosin (H&E) and Masson's trichrome (MT), and immunohistochemistry (IHC) stained with inflammation-related IL-6 and TNF-α, angiogenesis-related VEGF-A and TGF-β1, and osteogenesis-related OPN and ALP antibodies, followed by statistical analysis.

Results

S. aureus infected osteomyelitis model was successfully created in a rat mandible. Most parameters showed significantly lower bone healing in the C1 and C2 groups in micro-CT analysis. Especially in the E2 group, bone mineral density with bone volume was significantly enhanced compared to that seen in the C1 or C2 groups, and bone volume/volume of interest parameter was significantly higher ($p < 0.05$) in the E2 group. In the histological analysis, the E1 and E2 groups showed the most prominent bone healing with a significantly high number of osteocytes found in the defect area ($p < 0.05$). In IHC staining, the E2 group had the weakest expression of IL-6 compared to that of the C1 group. The TNF-α antibody was stained strongly in the E1 group compared to that of other groups. The expression of VEGF-A was the highest in the C1 group compared to the E2 group. The TGF-β1, ALP, and OPN expressions were markedly high in the E1 group,

while the C1 group had no TGF-β1, ALP, and OPN expression compared to that of the other groups.

Conclusion

The micro-CT, H&E, and MT stained histological analysis, and IHC analyses showed that decompression drains exhibited superior bone healing results compared with that of conventional surgical treatment alone in an OM rat mandible model. Based on these results, it is recommended that clinicians use decompression with drainage and irrigation to treat jaw OM.

Keywords: Osteomyelitis of jaw, *Staphylococcus aureus*, decompression, drainage, micro-CT, histology, IHC

Student Number: 2019-29083

Contents

I. Introduction

Osteomyelitis (OM) of the jaw is an inflammatory process that starts in the medullary space of the bone and progresses to cortical bone, the Haversian system, periosteum, and overlying soft tissue. This is usually caused by micro-organism infection into the bone tissues due to a trauma or odontogenic infection [1]. The gram positive pathogen *Staphylococcus aureus* (*S. aureus*) is the most common OM causative agent in both children and adults [2]. Other reasons include steroids, chemotherapeutic drugs, and bisphosphonates, which have been linked to jaw OM [3].

OM of the jaw is classified as acute and chronic, differentiated arbitrarily based on the time of onset and clinical presentation. An acute process occurs up to one month after the onset of symptoms and the chronic process occurs after more than one month [4]. Two different types of chronic OM are described in the literature, the suppurative type with the presence of pus and /or fistulas and/or sequestrations and the non-suppurative type, which are chronic inflammatory processes with an unexplainable onset, occasionally of unknown origin [5].

The treatment of jaw OM in the literature is classified as surgical and non-surgical, while the aim differs depending whether or not bacterial infection is apparent [5]. The universally acknowledged and effectual treatment is a combination of antibiotic therapy and surgery consisting of sequestrectomy, saucerization, decortication, and closed-wound suction irrigation [6]. The surgical therapy approach has major goals: 1) Decompression of the intramedullary pressure caused by the osteomyelitic effect and drainage of subperiosteal abscesses; 2) Surgical

treatment of infected tissue and removal of infectious foci; 3) Grafting healthy and well-perfused bone tissue into the infected area [7].

Animal models for *in vivo* testing of potential therapeutic approaches for OM have produced helpful results. To study jaw OM, animal species that include rats, rabbits, and pigs are considered to be the most suitable options [8]. Therefore, a number of different animal models that have studied *S. aureus*-induced OM have been reported in the literature [9,10], but there has been no study on the decompression effects of using a drain and irrigation for jaw OM in a rat model.

By definition, decompression is a technique that creates a small opening in the cystic wall for drainage that releases intraluminal pressure that causes cystic reduction and permits gradual bone growth from the periphery. This technique has been associated with minimal surgical morbidity, changes in the malignancy environment, prevention of reestablishment of intraluminal pressure, decrease or inhibition of the expression of interleukin (IL) 1α and IL-6 inside odontogenic cysts, maintenance of pulp vitality, preservation of anatomical structures, prevention of pathologic fracture, thickening of the cystic lining, and relatively low risk of recurrence [11].

Surgical drains are used for decompression effects, to eliminate pooled blood, serum and edema reduction, exudate management, and dead space reduction of the surgical wound by drawing the separated surfaces together [12]. These interventions are classified as open and closed with the latter one subdivided as passive or active. Active negative pressure drainage, also known as vacuum-assisted wound closure or negative-pressure wound therapy is a popular method for wound care including limb wounds, soft-tissue defects, chronic OM, osteofascial compartment syndrome,

amputation, and replantation. Past research results have shown the effects of using negative pressure wound therapy in the head and neck region that include decreased healing time, less pain, and full drainage effects [13]. Despite the increasing number of studies of decompression, there are no reported studies of decompressive effects using drains in the management of jaw OM.

The hypothesis of this study was that decompression is more effective with regard to bone healing for the treatment of jaw OM compared with conventional surgical treatment alone. The aim of this study was to investigate the effectiveness of decompression using a drain compared to management without drainage in a rat model of *S. aureus*-induced OM using micro-computed tomography (micro-CT) and histopathological analysis.

II. Materials and Methods

II.1. Establishment of an *S. aureus*-infected jaw osteomyelitis model in rat

Fourteen 8-week-old SPF Sprague-Dawley rats (OrientBio Inc., Seongnam, Korea) with an average weight of 230.13±13.87 g were used in our study. All the experimental protocols were reviewed and authorized by the Seoul National University (SNU) Institutional Animal Care and Use Committee (SNU-121123-12-11) and Institutional Biosafety Committee of SNU (SNUIBC-R121226-1-6). All procedures were in accordance with the "Recommendations for handling of Laboratory Animals for Biomedical Research" and complied with the Committee on Safety and ethical Handling Regulations for Laboratory Experiments at SNU. The animal experiment was conducted at the Institute for Experimental Animals, College of Medicine, SNU, in a laboratory infection room classified as for high risk infection studies or infectious studies that use experimental animals (Animal Biosafety Level 2: ABL 2). All animals were maintained in an individually ventilated 12-hour light/dark cycle cage system with the temperature ranging from 20-26 °C (23±3 °C), and were provided rodent food and water ad libitum. A schematic timeline of the experimental design is presented in Figure 1.

The bacterial strain used in our study was *S. aureus*, the most common causative pathogen for jaw OM [14]. We used a 2°C to 8°C freeze-dried *S. aureus* subsp. *Aureus* (ATCC® 29213, Manassas, VA, USA) and a Wichita designated clinical isolate that was provided by the Korean Culture Center of Microorganisms (KCCM®, Seoul, Korea).

The freeze dried culture was thawed via gentle agitation in a normal growth water bath for approximately 2 minutes. The surface of the freeze dried ampoule was then disinfected with 70% ethanol. The top glass vial was opened and 1 ml of sterile distilled water was added to evenly seal it. The suspended sample containing the *S. aureus* strain was then inoculated and spread with the spread method into a tryptic soy agar (TSA, BD Difco™, New Jersey, USA) plate medium using a sterilized inoculation loop and cultured in an incubator for 24 hours at 37°C. After incubation, a visible colony of *S. aureus* formed.

To determine bacterial density, we included two methods for monitoring the number of bacteria. Each method has its strengths and weaknesses, and therefore we used the direct method of plate count technique (PCT) and the indirect method of turbidometry [15]. The number of bacterial inoculation was determined by PCT, in which the number of colonies formed on the plate medium is proportional to the live bacteria contained in the sample, and the dilution ratio and the number of colonies are calculated by stepwise dilutions.

In the turbidity measurement, as the concentration of bacteria increases, the turbidity (absorbance) increases proportionally, therefore in order to measure turbidity as the actual number of bacteria, a correlation must be obtained. This can be obtained by measuring the number of bacteria with the direct plate count technique in parallel. The bacterial colony was harvested and was washed two times with 1 x PBS by vortexing and by centrifuge. The suspended *S. aureus* solution was transferred to a new glass cuvette containing 1xPBS and was adjusted to an optical density (OD) of 0.8 using a UV/VIS spectrophotometer (Spectrophotometer, PerkinElmer®, MA, USA) at 600 nm with a clear PBS solution as a control (Figs.

2a-b). For the study, the TSA culture was diluted by 4 different OD values in four steps: (OD=0.2) $1.1X10^6$; (OD=0.4) $2.0X10^6$; (OD=0.6) $4.5X10^6$; (OD=0.8) $1.1X10^7$. The bacterial inoculation was then determined to be (600 nm = OD0.8) $1x10^7$ CFU/ml, as the optimal bacterial amount required to induce jaw OM (Fig. 2c).

In the first stage of the experiment, infection with *S. aureus* was performed using a local inoculation route by injecting the bacterial suspension through the created defect [15]. The inoculation procedure was performed under general anesthesia using 90 mg/kg ketamine (50 mg/ml) (ketamine hydrochloride®; Yuhan Co., Seoul, Korea) + 10 mg/kg xylazine (23.32 mg/ml) (Rompun®; Bayer Korea, Ansan, Korea) that was administered intraperitoneally. The preparations for the surgical procedure including the skin preparation, disinfection, and draping were all performed according to standard protocols. An approximately 12 mm full-thickness longitudinal extra-oral incision was made parallel to the inferior border of the right and left side of rat mandibles. Adequate subcutaneous, deep fascial and periosteal dissections were performed followed by retraction with forceps. Using a low-speed hand piece with 1.2 mm diameter round bur, a bilateral circular 4 mm defect was created in the rat mandible with copious irrigation. Considering the anatomy of the rat and the objective of the study, a circular 4 mm defect is a generally accepted mandibular bone defect [16]. All animals received 20 µl of 10^7 CFU/ml *S. aureus* injection into the defect and were covered with Greenplast kit® fibrin glue (Greencross Co., Yongin, Korea). The surgical wound was then carefully sutured at the subcutaneous layer with resorbable 4-0 Vicryl® (Polyglactin 910®, Johnson & Johnson Co., NJ, USA) sutures and the skin closure was performed using silk sutures (Black silk®, 4–0; AILEE Co., Busan, Korea) as shown in Figures 3a-l.

II.2. Grouping and experimental design

In the second stage of the study, the animals were randomly divided into control (non-decompression groups, C1 and C2) and experimental groups (decompression groups, E1 and E2) (Table 1). The C1 group (n=3) served as the control group, who only received wound closure. The C2 control group (n=4) received conventional surgical curettage for jaw OM.

The experimental groups were further classified into two subgroups, E1 group (n=3), which received removal of pus and necrotic bone tissue and curettage, followed by introducing the tube drain and E2 group (n=4), which received removal of pus and necrotic bone tissue and curettage, drain insertion and irrigation with normal saline every week (Figs. 4c-l).

Blood samples were collected from the tail vein pre-infection, 1-week post-infection, 2-weeks post-infection/the start of the treatment, 1-week after treatment, and 4-weeks after the treatment, and rat weights were checked (Figs. 4a-b).

Surgical treatment was performed under general anesthesia as previously described. Three mm in diameter silicone tubes that were approximately 3 cm in length (Daihan scientific Co. Ltd., Wonju, Korea) were used as a drain. The length of the tube was adjusted to each animal according to the post-curettage conditions and these were sutured in place using 4-0 silk sutures. To keep the tubes intact and in place, we used a plastic collar to prevent scratching and accidental displacement of the draining tubes.

Upon the completion of the six-week experimental trial, the animals were euthanized by CO_2 inhalation. The mandibles of the rats were immediately harvested and carefully isolated.

II.3. The analysis of bone healing with Micro-CT

A total of 16 excised rat mandible specimens were subjected to high-resolution micro-CT scanning Skyscan 1172® (Bruker, Kontich, Belgium). The scanning parameters of the source were adjusted to an Al filter of 0.5 mm, source voltage of 70 kV, source current of 141 µA, and 360° rotations at 0.4° rotation steps. This resulted in images that were 496 pixels in width and 900 pixels in height that were used for two-dimensional and three-dimensional (3D) analyses.

Following the scanning procedure, the raw data sets were reconstructed using NRecon 1.6.9.8® (Bruker, Kontich, Belgium) software. The smoothing was adjusted to 6, ring artifact correction to 7, with a beam hardening correction to 10%.

Each dataset was opened and further adjusted using DataViewer® (Bruker, Kontich, Belgium) software. The region of interest (ROI) were determined in the sagittal plane and the image analysis were performed using CTAn software® (version 1.18.4.0, Bruker, Kontich, Belgium). Incisor roots were excluded from the analysis and only bone tissue was included for bone analysis. Equivalent thresholds were adjusted in all images. To determine the ROI, a 4 mm wide circular area was set up in the sagittal plane where the initial 4 mm bone defect area could be seen. For optimal comparison between the samples, an identical number of slices were selected. Four square shaped ROI's were defined as 1.0 mm in width and 1.0 mm in height that were adjusted for analysis at the center and the inferior borders of the circular area as seen in Figure 5. The same procedure was performed on the contralateral rat mandible. Within the ROI, bone mineral density (BMD, g/cm^3), bone volume (BV, mm^3), and bone volume/volume of interest (BV/VOI, %), bone surface (BS, mm^2), bone surface/volume ratio (BS/BV, 1/mm), trabecular thickness (TB.Th., mm),

trabecular number (Tb.N, 1/mm), and trabecular separation (Tb.Sp., mm) were measured and compared. The datasets were reconstructed into 3D images using CTvox volume rendering software® (Bruker MicroCT, Kontich, Belgium).

II.4. The histological and immunohistochemical analysis of OM healing

The samples from each group were trimmed and decalcified with 0.5 M ethylene diamine tetra-acetic acid EDTA® (pH 8.0) (Biosesang, Seongnam, Korea) solution for ten days, dehydrated with 70% ethanol, and embedded in paraffin wax. The sections were then cleaned with xylene for approximately 10 minutes and 4 μm thick slides were stained with hematoxylin and eosin (H&E) and Masson's trichrome (MT). The histological slides were then scanned with a 3D Scan Panoramic Histech scanner® (3D HistechKft. Budapest, Hungary) and examined using CaseViewer® (version: 2.0, 3DHISTECH, Budapest, Hungary).

For quantitative analysis, the number of osteocytes within the regenerated bone tissues of the defect area were counted. An area of interest using a fixed rectangular form of 350 x 300 μm within the initial defect area where the bone tissues were regenerated was established by the histological imaging program CaseViewer® (version: 2.0, 3DHISTECH, Budapest, Hungary) in all of the specimens at a magnification of 20x (Fig. 6).

Decalcified and paraffin-embedded samples were cut into standardized 4 μm intervals and were collected in serial sections mounted on glass slides for IHC staining with an automated BOND-MAX system® (Leica Microsystems, Mannheim, Germany). The slides were examined using a BX41® Light Microscope (Olympus Co., Tokyo, Japan). For IHC staining we used vascular endothelial growth factor A

(VEGFA) (1:100, ab46154, Abcam, Cambridge, MA, USA), Transforming growth factor β1 (TGFβ1) (1:100, sc-130348, Santa Cruz Biotechnology, Santa Cruz, CA, USA), Osteopontin (OPN) (1:100, sc-73631, Santa Cruz Biotechnology, Santa Cruz, CA, USA), Alkaline Phosphatase (ALP) (1:100, sc-271431, Santa Cruz Biotechnology, Santa Cruz, CA, USA), tumor necrosis factor-α (TNF-α) (1:100, 300-01A, PeproTech, New Jersey, USA) and interleukin-6 (IL-6) (1:100, sc-28343, Santa Cruz Biotechnology, Santa Cruz, CA, USA) antibodies. The staining was scored as follows: "1": none, "2": 1–25%, "3": 26–50%, "4": 51–75%, and "5": 76–100% cells stained [17]. The intensity of the antibody staining was assessed using a previously described method [18].

II.5. Statistical analyses of Micro-CT and histological data of bone healing

Means and standard deviations (SDs) for bone healing parameters were obtained. Data normality by variable was assessed using the Shapiro-Wilk test and the differences were tested by Student's t-test and one-way ANOVA followed by post hoc Scheffé test for multiple comparisons. Statistical analyses were done using SPSS 25.0® (SPSS Software Company, Chicago, USA). P values < 0.05 were considered statistically significant.

III. Results

III.1. Establishment of an *S. aureus*-infected jaw osteomyelitis model in rat

After two weeks of infection, all groups showed visible infectious jaw OM including: skin redness, swelling, and alopecia. The pathogen dose of 20 µl of 10^7 CFU/ml was effective in creating jaw OM in the rat model and a repeatable animal model was established. Six animals died during the experimental trial and were excluded from this study.

III.2. Clinical evaluation with blood test

After the infection with *S. aureus* all animals from the control and the experimental groups showed weight loss (Table 2). Significant weight loss in all groups was observed with an average of -31.57±21.98 g at one week after the infection that was recovered after two weeks ($p < 0.05$). A statistically significant difference was observed between the groups at 1 week after treatment ($p < 0.05$) (Fig. 7).

The neutrophil count was significantly increased after the infection in all groups. There were no statistically significant differences in neutrophil count between the groups at one week and four weeks after treatment. The white blood cell count (WBC) was significantly increased in all groups after infection and was recovered to the normal range at four weeks after treatment. No significant differences were observed between the groups at one week after treatment and four weeks after treatment (Table 4). Serum levels of alkaline phosphatase (ALP) were also measured and analyzed. At one week after infection, ALP levels were significantly increased in all groups

and a significant reduction was observed at one week and two weeks after treatment. No significant differences were found between groups (Table 5).

III.3. Micro-CT results of bone healing

From the 3D images, more bone healing was observed in the E1 and E2 groups, where the initial bone defect was replaced by new bone tissue. The E2 group had the most compact bone formation compared to the other groups.

The BMD results were significantly different between the groups. The BMD in the C1 group was significantly lower compared to that of the E1 and E2 groups, with a mean difference of -0.29 and -0.45 respectively ($p < 0.05$). The BMD in the E2 group was 0.87±0.16 g/cm^3, which was significantly higher compared to that of the control groups ($p < 0.05$) (Table 6) (Fig. 8a).

The BV parameter was highest among the experimental groups. The E1 group showed significantly higher results compared to that of the C1 group ($p < 0.05$), while the E2 group was significantly higher compared to that of the control groups with a mean value of 0.73±0.17 mm^3 ($p < 0.05$) (Fig. 8b). The BV/VOI parameter was significantly higher in the E2 group, with an average value of 75.70±14.32 % compared to that of the control groups (Fig. 8c). The BS, BS/VOI, Tb.N, Tb.Sp parameters were significantly different between the control and experimental groups (Table 7). Most bone healing parameters were lower in the control groups compared to the experimental groups (Figs. 9a-c). However, the Tb.Sp parameter in the C1 group was significantly higher than that in the experimental groups (Fig. 9d). The BS/BV parameter in C2 was the highest among the groups at 25.18±13.26 1/mm. The Tb.Th parameter was not significantly different between the groups.

III.4. Histological and immunohistochemical results of OM healing

The morphological changes in bone healing were macroscopically observed in the H&E and MT stained slides at 4-weeks in the defect area.

The C1 group showed high grade inflammatory infiltration consisting of neutrophils, eosinophils, and macrophages around the bacterial colonies. Signs of infective osteomyelitis including bone necrosis, bone resorption and destruction, with no bone healing were observed (Figs. 10a1-a3). In MT staining, the C1 group were stained with thick blue color, indicating old bone, while no new bone formation stained with bright blue color were observed (Figs. 11a1-a3). Histological findings for the C2 group showed bone healing with osteoblastic cell lining in the parenchymal tissue found at the center of the defect area with evidence of inflammatory infiltrates (Fig. 10b1-b3, 11b1-b3).

The histology features of the E1 group included loose marrow fibrosis and scattered lymphocytic inflammatory infiltrates. In the MT stain, new bone formation stained with bright blue color and new blood vessels were observed (Figs. 10c1-c3, 11c1-c3). The E2 group showed active bone remodeling with the thickest and most compact new bone formation being in the defect area compared to that of other groups. Increased osteophytic bone formation was observed. Furthermore, an increased number of Haversian canals with osteoblast rimming and new blood vessel formation stained with thick red color by the MT stain were seen (Figs. 10d1-d3, 11d1-d3).

For the quantitative analysis, we counted the number of osteocytes and Haversian canals in the ROI. The results showed that the E2 groups had a statistically

significant greater osteocyte count compared to the control groups ($p < 0.05$) (Table 8).

In order to confirm the inflammatory, angiogenic, and osteogenic properties in the control and experimental groups, IHC staining was performed. The expression of inflammation-related antibody IL-6 in the E2 group was weak (score "2": 1–25% of cells positive), compared with that of the C1 group ("5": 76–100% cells stained) (Figs. 12a1-d2). The TNF-α antibody stained strongly in the E1 group compared to that in the other groups ("5": 76–100% cells stained) (Figs. 13a1-d2).

The expression of VEGF-A was the highest ("5": 76–100%) compared to that of E2 ("2": 1–25%) (Figs. 14a1-d2). TGF-β1 expression was markedly high in the E1 group, while the C1 group showed no expression ("1": none) (Figs. 15a1-d2). The osteogenesis markers, ALP and OPN, were also strongly expressed in the E1 group compared to that seen in other groups (Figs. 16a1-d2, 17a1-d2).

IV. Discussion

In spite of improvements in medical and dental care, jaw OM is still a common disease, which poses diagnostic and therapeutic issues even to an experienced oral and maxillofacial surgeon, because this disease can lead to potential functional impairment and permanent disability [19]. With the introduction of antibiotics, the threat of acute jaw OM has decreased significantly, however recurring and persistent jaw OM are still major concerns for clinicians [20].

The standard regimen for jaw OM treatment has been well established in the scientific literature, which consists of early diagnosis, elimination of infection source, establishment of surgical drainage, bacteriological identification, antibiotic therapy, surgical treatment, supportive treatment, and lastly reconstruction [21]. There are a variety of conventional treatment options that include antibiotics, nonsteroidal anti-inflammatory drugs, and hyperbaric oxygen therapy that is used as an adjunctive treatment, but the disease still has a high recurrence rate and life-threatening complications [1,22]. Therefore, it is important to establish an effective treatment method for jaw OM.

In the oral and maxillofacial surgery field, evidence suggests that active and passive decompression promotes osteogenesis, stimulates angiogenesis, creates short-term hypoxia, and exerts forces capable of removing the cystic lining and its contents as a definitive treatment for odontogenic cysts of the jaw [11]. According to an observational study by Lin *et al*., negative pressure drainage for oral and maxillofacial surgery patients found that its application can hasten wound healing, decrease hospital stay length, improve patient comfort, and decrease clinician

workload [23]. Also, an animal study by Zhang *et al.* found that intermittent negative pressure reduced bone healing time and enhanced bone regeneration by enhancing the expression of VEGF and bone morphogenetic protein 2 [24]. Nakahashi *et al.* reported that closed continuous irrigation-suction treatment was effective not only for chronic suppurative jaw OM but also for the more intractable sclerosing type of OM after following complete removal of the affected tissues [25]. Based on our current animal study and previous reports, decompression effects with drainage have several important therapeutic effects including reduced treatment time, enhanced bone regeneration, and reduced complication and recurrence rates.

The significance of this study is that it demonstrates the effectiveness of decompression using a drain in jaw OM, which had significant bone healing effects according to micro-CT, histology, and IHC analyses. To our knowledge, there are no scientific data in the literature on decompression effects using a drain in jaw OM.

We established an *S. aureus*-infected OM of the mandible in a rat model to study the bone healing properties of decompression using a drain for jaw OM. The OM induced in our study is classified as infectious jaw OM, as *S. aureus* colonization was induced by injection in a created mandibular defect. The current animal model has shown it is a repeatable and reproducible OM of the mandible in a rat model based on clinical, laboratory, and histological findings. This rat model has not been described in the literature before.

The mechanisms of decompression and drainage in bone healing can be explained by fluid removal and alteration of the wound environment to be conducive to healing. Excess fluid build-up is regarded as one of the major factors that compromise healing, partly owing to the compressive pressure that it exerts on local

cells and surrounding tissue. Each cell has an intrinsic tension exerted by the interactions between its cytoskeleton and the extracellular matrix, that induce a proliferative response. If the fluid pressure is elevated in the interstitium, the proliferative response diminishes due to dampened intrinsic tension buildup. The fluid from the extracellular space is thought to communicate with the wound surface. Applying decompression and drainage to this area permits fluid removal from the extracellular space [26]. The removal of postoperative fluid allows decompression of the microvasculature that permits tissue perfusion by reducing pressure and enhancing blood circulation to the area. It will also remove the toxins, inflammatory exudate, and pathogenic bacteria from the operative site, which is considered to be an important element in the wound healing process.

Micro-CT analysis tools provided highly reproducible methodology with qualitative and quantitative assessment of bone microstructure. Micro-CT is considered to be a gold standard method for assessing mineral density, bone morphology, and bone micro-architecture under various pathologic conditions [27,28]. We report our methodology according to the guidelines for assessment of bone microstructure in rodents using micro-CT [29] and results by following morphometric indices that can determine new bone formation [30]. The most informative parameters which show the course of bone healing are BV, BV/VOI, BS/BV, and BMD [28,30]. The BV/VOI in the E2 group showed a mean value of 11.44±2.68 %, indicating the highest amount of bone regeneration that was significantly higher than that seen in the control groups. The Tb.N was the highest in the E2 group at 3.18±1.101/mm, while the Tb/Sp was lowest among all the other groups at 0.13±0.06 mm, indicating more bone closure. The volume of mineralized

bone tissue was the highest in the E2 group at 0.73±0.16 mm^3, which was significantly higher than that seen in the control groups. Bone healing is characterized by a gradual increase in BV, BMD, and a decrease in BS/BV, and the volume of pore space. The E1 and E2 groups had the highest values for BV and BMD, and a decreased value for BS/BV. The 3D evaluation showed more rapid bone healing was detected in the E1 and E2 groups compared to that of the positive control group C2 (Figs. 18a-d). Micro-CT analysis showed more favorable outcomes in bone healing after decompression treatment.

Although micro-CT analysis is a nondestructive method for assessing internal and external bone morphology with high resolution and high accuracy, it has significant weaknesses compared to histomorphometric study, as it does not reveal cell proliferation and differentiation, vascularization, microcirculation inside the bone, or the rate of mineral apposition and bone remodeling [28]. Therefore, we performed histological and IHC studies to evaluate the angiogenic, osteogenic, and inflammatory state after decompression. In terms of bone healing and anti-inflammation, the experimental groups showed more effective results that included rapid bone healing, blood vessel formation, and reduced inflammation. The E2 group also had the highest osteocyte count. An increase in osteocytes plays a pivotal role in regulating bone turnover, which also enhances osteogenesis of stem cells, suggesting an important role in tissue regeneration [31]. The histological results suggested the most optimal bony healing was seen in the experimental groups, which is in accordance with the micro-CT analysis.

VEGF-A is thought to play an important role in regulating angiogenesis as well as bone development and regeneration. Angiogenesis and osteogenesis are two

intimately connected processes that must be closely coupled to permit physiological bone function. In fact, alterations in vascular growth can alter the physiological bone healing process, which may lead to osteoporosis, osteonecrosis, and non-union fractures [32]. According to a previous clinical study, decompression had a direct influence on the microvascular circulation, and enhanced VEGF-A protein in the first day following surgical treatment, thereby activating osteogenesis-related proteins that included OPG and ALP that were decreased on the second day [33]. In our study we demonstrated that VEGF-A was activated and reduced in the E2 group, leading to enhanced and accelerated bone healing compared to the E1 group, while bone healing was evident, but much slower.

IHC staining showed the pro-inflammatory antibodies IL-6 and TNF-α were strongly stained in the C1 group, indicating an inflammatory reaction to the bacteria, while the groups which received surgical treatment were weakly stained, except in the E1 group, where TNF-α was strongly stained. In the bone remodeling phase, TNF-α and other pro-inflammatory cytokines are thought to play an important role in bone healing [34]. These osteogenesis-related antibodies were also strongly stained in the E1 group, suggesting an active and highly controlled bone resorption and bone regeneration process in the decompression group. On the other hand, the, the E2 group showed very rapid bone proliferation with decreased bone marrow space compared to the E1 group.

V. Conclusion

The results were in accordance with our hypothesis that decompression using a drain had significant therapeutic effects on bone regeneration for jaw OM. When decompression was applied to the curettage treatment, enhanced wound and bone healing were achieved. The decompression effects on the healing process were much enhanced with weekly normal saline irrigation.

Therefore, it could be recommended to implement decompression using a drain as a treatment in combination with surgical treatment to allow accelerated bone healing.

Reference

1. Chen L, Li T, Jing W, Tang W, Tian W, Li C, Liu L. Risk factors of recurrence and life-threatening complications for patients hospitalized with chronic suppurative osteomyelitis of the jaw. BMC Infect Dis. 2013;13(1):313.

2. Cassat JE, Skaar EP. Recent advances in experimental models of osteomyelitis. Expert Rev Anti Infect Ther. 2013;11(12):1263-5.

3. Dym H, Zeidan J. Microbiology of acute and chronic osteomyelitis and antibiotic treatment. Dent Clin North Am. 2017;61(2):271-82.

4. Patel V, Harwood A, McGurk M. Osteomyelitis presenting in two patients: a challenging disease to manage. Br Dent J. 2010;209(8):393-6.

5. Gudmundsson T, Torkov P, Thygesen T. Diagnosis and treatment of osteomyelitis of the jaw – a systematic review (2002-2015) of the literature. J Dent & Oral Disord. 2017;3:1066.

6. Bennett J, Dolin R, Blaser M. Mandell, Douglas, and Bennett's principles and practice of infectious diseases. Osteomyelitis. 2020. p. 1418-29.

7. Baltensperger M, Eyrich G. Osteomyelitis of the jaws: definition and classification. Osteomyelitis of the jaws. 2009. p. 5-56.

8. Patel M, Rojavin Y, Jamali AA, Wasielewski SJ, Salgado CJ. Animal models for the study of osteomyelitis. Semin Plast Surg. 2009;23(2):148-54.

9. Haenle M, Zietz C, Lindner T, Arndt K, Vetter A, Mittelmeier W, Podbielski A, Bader R. A model of implant-associated infection in the tibial metaphysis of rats. Sci World J. 2013;2013:481975.

10. Horst SA, Hoerr V, Beineke A, Kreis C, Tuchscherr L, Kalinka J, Lehne S, Schleicher I, Köhler G, Fuchs T, Raschke MJ, Rohde M, Peters G, Faber C, Löffler B, Medina E. A novel mouse model of Staphylococcus aureus chronic osteomyelitis that closely mimics the human infection: an integrated view of disease pathogenesis. Am J Pathol. 2012;181(4):1206-14.

11. Castro-Núñez J. Distraction sugosteogenesis: its biologic bases and therapeutic principles. J Craniofac Surg. 2018;29(8):2088-95.

12. Flynn TR, Hoekstra CW, Lawrence FR. The use of drains in oral and

maxillofacial surgery: a review and a new approach. J Oral Maxillofac Surg. 1983;41(8):508-11.

13. Qiu Y, Li Y, Gao B, Li J, Pan L, Ye Z, Lin Y, Lin L. Therapeutic efficacy of vacuum sealing drainage-assisted irrigation in patients with severe multiple-space infections in the oral, maxillofacial, and cervical regions. J Craniomaxillofac Surg. 2019;47(5):837-41.

14. Fukushima N, Yokoyama K, Sasahara T, Dobashi Y, Itoman M. Establishment of rat model of acute staphylococcal osteomyelitis: relationship between inoculation dose and development of osteomyelitis. Arch Orthop Trauma Surg. 2005;125(3):169-76.

15. An YH, Kang QK, Arciola CR. Animal models of osteomyelitis. Int J Artif Organs. 2006;29(4):407-20.

16. Dong QN, Kanno T, Bai Y, Sha J, Hideshima K. Bone regeneration potential of uncalcined and unsintered hydroxyapatite/poly l-lactide bioactive/osteoconductive sheet used for maxillofacial reconstructive surgery: An in vivo study. Materials (Basel). 2019;12(18):2931.

17. Meyerholz DK, Beck AP. Principles and approaches for reproducible scoring of tissue stains in research. Lab Invest. 2018;98(7):844-55.

18. Zhang B, Sun Y, Chen L, Guan C, Guo L, Qin C. Expression and distribution of SIBLING proteins in the predentin/dentin and mandible of hyp mice. Oral Dis. 2010;16(5):453-64.

19. Andre CV, Khonsari RH, Ernenwein D, Goudot P, Ruhin B. Osteomyelitis of the jaws: a retrospective series of 40 patients. J Stomatol Oral Maxillofac Surg. 2017;118(5):261-4.

20. Goda A, Maruyama F, Michi Y, Nakagawa I, Harada K. Analysis of the factors affecting the formation of the microbiome associated with chronic osteomyelitis of the jaw. Clin Microbiol Infect. 2014;20(5):O309-17.

21. Koorbusch GF, Deatherage JR, Curé J. How can we diagnose and treat osteomyelitis of the jaws as early as possible? Oral Maxillofac Surg Clin North Am. 2011;23 4:557-67.

22. Urade M, Noguchi K, Takaoka K, Moridera K, Kishimoto H. Diffuse sclerosing osteomyelitis of the mandible successfully treated with pamidronate: a long-term

follow-up report. Oral Surg Oral Med Oral Pathol Oral Radiol. 2012;114(4):e9-e12.
23. Lin Y, Wang H, Zhang X. Application of vacuum sealing drainage in oral and maxillofacial surgery. Biomed Res. 2018;29:628-32.
24. Zhang Y-g, Yang Z, Zhang H, Liu M, Qiu Y, Guo X. Negative pressure technology enhances bone regeneration in rabbit skull defects. BMC Musculoskelet Disord. 2013;14(1):76.
25. Nakahashi K, Horiuchi K, Fujimoto M, Inada I, Hyomoto M, Morimoto Y, Sugimura M. Closed continuous irrigation-suction treatment for chronic osteomyelitis of the mandible. Int J Oral Maxillofac Surg. 1997;26:147.
26. Huang C, Leavitt T, Bayer LR, Orgill DP. Effect of negative pressure wound therapy on wound healing. Curr Probl Surg. 2014;51(7):301-31.
27. Faot F, Chatterjee M, de Camargos GV, Duyck J, Vandamme K. Micro-CT analysis of the rodent jaw bone micro-architecture: A systematic review. Bone Rep. 2015;2:14-24.
28. Kustro T, Kiss T, Chernohorskyi D, Chepurnyi Y, Helyes Z, Kopchak A. Quantification of the mandibular defect healing by micro-CT morphometric analysis in rats. J Craniomaxillofac Surg. 2018;46(12):2203-13.
29. Bouxsein ML, Boyd SK, Christiansen BA, Guldberg RE, Jepsen KJ, Müller R. Guidelines for assessment of bone microstructure in rodents using micro-computed tomography. J Bone Miner Res. 2010;25(7):1468-86.
30. Kallai I, Mizrahi O, Tawackoli W, Gazit Z, Pelled G, Gazit D. Microcomputed tomography–based structural analysis of various bone tissue regeneration models. Nat Protoc. 2011;6(1):105-10.
31. Cao W, Helder MN, Bravenboer N, Wu G, Jin J, Ten Bruggenkate CM, Klein-Nulend J, Schulten EAJM. Is there a governing role of osteocytes in bone tissue regeneration? Curr Osteoporos Rep. 2020;18(5):541-50.
32. Grosso A, Burger MG, Lunger A, Schaefer DJ, Banfi A, Di Maggio N. It takes two to tango: coupling of angiogenesis and osteogenesis for bone regeneration. Front Bioeng Biotechnol. 2017;5(68).
33. Kim SM, Eo MY, Cho YJ, Kim YS, Lee SK. Immunoprecipitation high performance liquid chromatographic analysis of healing process in chronic suppurative osteomyelitis of the jaw. J Craniomaxillofac Surg 2018;46(1):119-27.

34. Mountziaris PM, Mikos AG. Modulation of the inflammatory response for enhanced bone tissue regeneration. Tissue Eng Part B Rev. 2008;14(2):179-86.

Tables

Table 1. Animal grouping. The animals were divided into control groups (C1 and C2) and experimental groups (E1 and E2).

Group	Treatment	Sacrifice period
C1	Non-decompression group, suturing after incision	4 weeks
C2	Non-decompression group, debridement of necrotic tissue and curettage	4 weeks
E1	Debridement of necrotic tissue and draining tube insertion after curettage	4 weeks
E2	Debridement of necrotic tissue and curettage followed by draining tube insertion and normal saline irrigation at 1-week intervals	4 weeks

Abbreviation: CFU: Colony Forming Unit.

Table 2. Weight changes after infection with *S. aureus* and treatment in the control and experimental groups.

Group	Before infection (g)	1 week after infection (g)	2 weeks after infection (g)	1 week after treatment (g)	4 week after treatment (g)
C1	223.63±4.12	190.40±11.47	210.15±42.78	211.90±40.58	245.75±4.03
C2	223.35±8.00	177.3±20.30	210.35±25.81	198.40	259.90
E1	246.80±19.47	209.45±5.63	237.45±2.19	243.30±7.07	275.30±19.37
E2	229.27±11.10	216.6±17.41	246.46±20.96	260.46±7.59	294.60±11.51

The weight changes are depicted as mean ± standard deviation.

Table 3. The change of the Neutrophil percentage

Group	Before infection	1week after infection	2weeks after infection	1week after treatment	4weeks after treatment
C1	12.20±3.11	33.45±4.45	29.26±7.82	32.50±3.53	13.00±4.94
C2	28.52±15.13	35.87±19.79	37.00±2.68	29.10	7.90
E1	22.75±15.12	30.36±5.71	20.60±4.10	34.40±9.30	12.77±4.08
E2	16.00±6.29	31.95±2.49	34.12±7.31	28.96±9.00	13.16±2.26

The changes are depicted as mean ± standard deviation.

Table 4. Changes of WBC count

Group	Before infection	1 week after infection	2 weeks after infection	1 week after treatment	4 weeks after treatment
C1	8.70±2.74	9.15±3.41	17.10±4.28	16.47±3.73	8.11±1.27
C2	7.51±0.57	12.52±3.05	17.43±9.01	13.37	9.65
E1	12.52±0.67	13.31±3.88	14.63±3.93	16.50±7.02	10.46±1.91
E2	11.19±2.39	17.01±7.61	20.09±3.42	18.38±4.50	11.77±0.62

The changes are depicted as mean ± standard deviation.

Table 5. Results of ALP changes

Group	Before infection	1 week after infection	2 weeks after infection	1 week after treatment	4 weeks after treatment
C1	535.33±77.50	957.66±185.30	957.31±957.31	526.00±42.42	389.50±6.36
C2	702.75±107.77	1512.25±267.35	1110.5±272.09	526.00	488.00
E1	817.00±179.67	1374.00±231.63	957.31±213.98	588.00±132.82	407.33± 65.63
E2	739.66±179.66	984.25±302.69	860.00±65.79	718.00±117.20	390.33±101.20

The changes are depicted as mean ± standard deviation (SD).

Table 6. Bone Mineral Density (BMD) measured at the osteomyelitis defect site.

	BMD (g/cm^3)				
Group	ROI (1)	ROI (2)	ROI (3)	ROI (4)	Total
C1	0.23±0.30	0.61±0.2	0.37±0.27	0.45±0.32	0.41±0.15
C2	0.16±0.01	0.84±0.16	0.39±0.47	0.72±0.19	0.53±0.30
E1	0.66±0.06	0.96±0.09	0.60±0.27	0.58±0.07	0.70±0.17*
E2	0.76±0.13	1.02±0.07	0.97±0.11	0.71±0.11	0.86±0.15**

The data is depicted as mean ± standard deviation. Abbreviation: ROI: Region of Interest. *E1 group was significantly higher than C1 ($p < 0.05$). *E2 group was significantly higher than C1 and C2 groups ($p < 0.05$).

Table 7. Micro-CT morphometric parameters of the bone regeneration area in 3D analysis

Group	BV (mm^3)	BV/VOI (%)	BS (mm^2)	BS/BV (1/mm)	BS/VOI (1/mm)	Tb.Th (mm)	Tb.N (1/mm)	Tb.Sp (mm)
C1	0.36±0.23	37.31±24.59	5.66±2.74	19.31±8.90	5.83±2.81	0.23±0.09	1.51±0.77	0.46±0.21
C2	0.45±0.32	46.26±32.58	7.91±4.02	25.18±13.26	8.04±4.08	0.17±0.07	2.23±1.18	0.34±0.29
E1	0.55±0.18	57.79±19.53	9.80±2.20	20.53±7.26	10.70±2.21	0.22±0.09	2.78±0.88	0.20±0.13
E2	0.73±0.16	75.70±14.32	11.07±2.82	17.69±10.73	11.44±2.68	0.27±0.12	3.18±1.10	0.13±0.06
P valu	0.00	0.00	0.00	0.32	0.00	0.24	0.00	0.00

The data is depicted as mean ± standard deviation. Abbreviation: BV: bone volume, BV/VOI: bone volume/volume of interest, BS: bone surface, BS/BV: bone surface/volume ratio, BS/VOI: bone surface/volume of interest ratio, Tb/Th: trabecular thickness, Tb.N: trabecular number, Tb.Sp: trabecular spaces ($p < 0.05$).

Table 8. Osteocyte and Haversian canal count in the ROI

Group	Osteocyte	Haversian canal
C1	60.5±10.1	5.75±3.30
C2	53.5±9.20	8.00±1.40
E1	77.25±8.40	8.50±2.90
E2	91.00±9.90*	9.75±2.10

The data is depicted as mean ± standard deviation. *The osteocytes found in the E2 group were significantly higher than in the C1 and C2 groups, ($p < 0.05$).

Figures and Figure legends

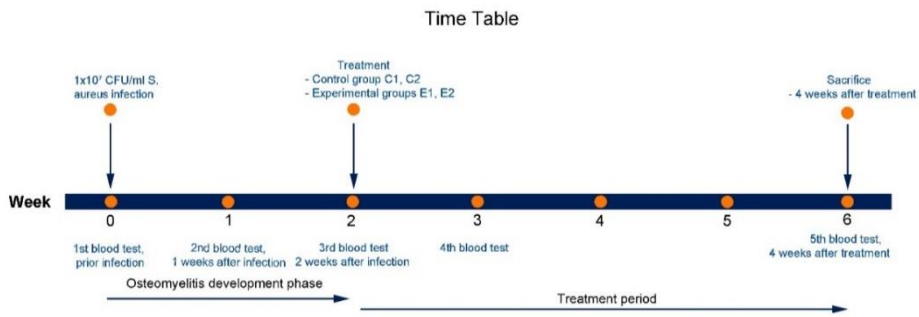

Figure 1. Schematic time table of the animal experiment.

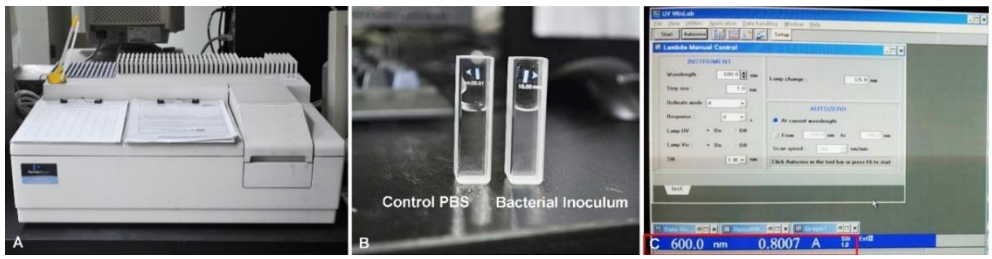

Figure 2. A UV/VIS spectrophotometer (Spectrophotometer, PerkinElmer®, MA, USA) adjusted to 0.8 OD at 600 nm was used to measure the bacterial density for infection (a-b). The bacterial inoculation was then determined to be (600 nm = OD 0.8) $1x10^7$ CFU/ml, as the optimal bacterial amount for developing jaw OM (c).

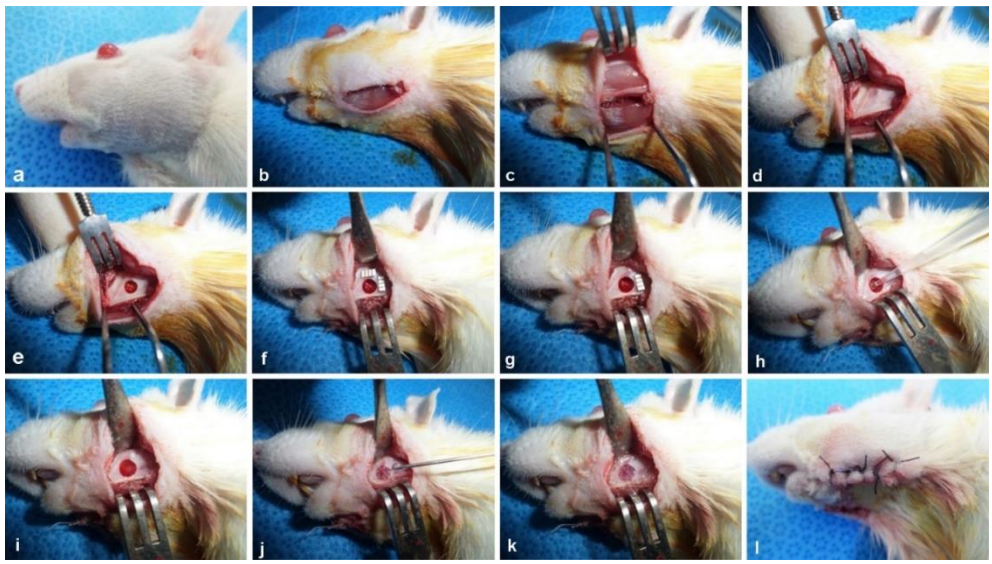

Figure 3. Creation of jaw OM in a rat model was performed by a local inoculation route by injecting the bacterial suspension through a hole (a 4 mm defect) in the rat mandibular bone (a-g). All animals received 10^7 CFU/ml, 20 µl *S. aureus* injection into the 4 mm circular mandibular bony defect that was created at the surgical site (a-h) and were covered with Greenplast kit® fibrin glue (Greencross Corp., Yongin, Korea) (i-k) and the subcutaneous layer was carefully sutured with resorbable 4-0 Vicryl® (Polyglactin 910®, Johnson & Johnson Co., NJ, USA) sutures and the skin closure was performed using silk sutures (Black silk, 4–0; AILEE Co., Ltd., Busan, Korea) (l).

Figure 4. The treatment procedure for the E2 group. Before the treatment, weights were measured (a-b). Two weeks after the *S. aureus* inoculation, the pus was first aspirated with a syringe and the necrotic tissue was removed (c-d). After complete debridement of the pathologic tissue, a decompression tube was then inserted and secured in place with sutures (e-j). The decompression E2 group received drainage and irrigation with NS treatment every 1 week (k-l).

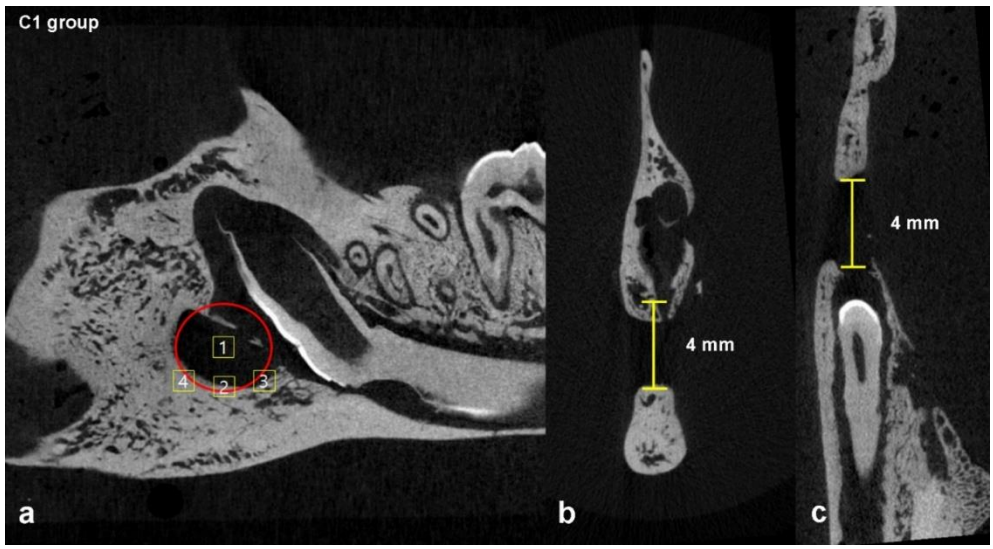

Figure 5. ROI designation method at the round 4 mm defect area. A circular area with a 4 mm wide diameter was first set in the sagittal plane that depicted the defect and four 1 x 1 mm square ROIs were set at the center of the defect and the inferior margins of the circular area (a). Coronal view showing the 4 mm bone defect (b). Axial plane showing bone defects and bone destruction at the buccal surface of the rat mandible (c).

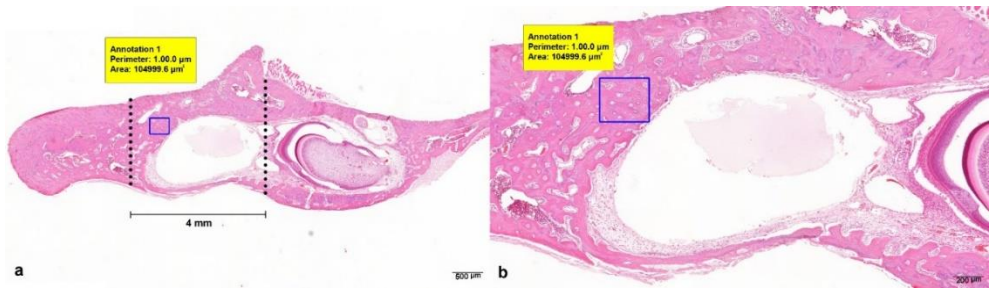

Figure 6. Osteocyte and Haversian canal count method, 2x (a). At the center of the defect area with bone regeneration, a 350 x 300 µm fixed rectangle was selected as the area of interest for counting, 5x (b).

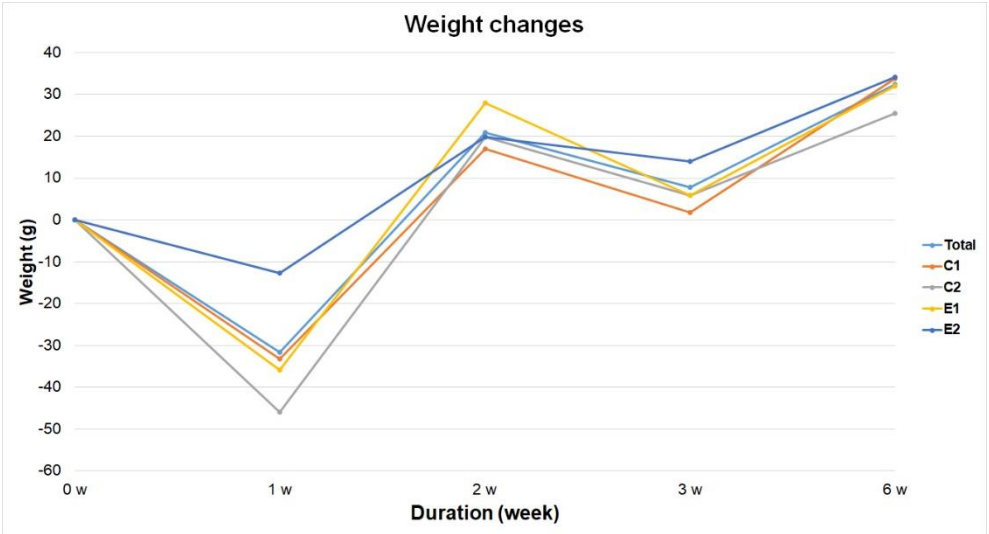

Figure 7. Graph depicting the weight change differences between the non-decompression and decompression groups.

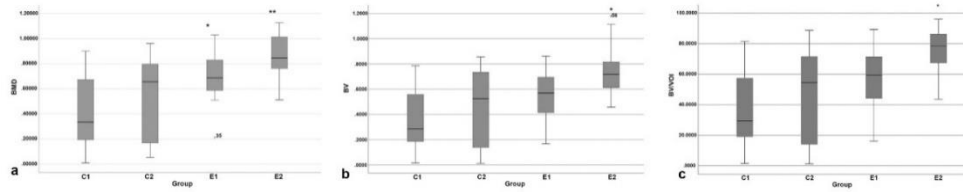

Figure 8. BMD differences between the groups. The E1 group was significantly higher than the C1 group (*p< 0.05). The E2 group was significantly higher than the C1 and C2 groups (**p< 0.05) (a). The BV and BV/VOI was significantly higher in the E2 group than in the control groups (*p< 0.05), while the E1 group showed no significant differences with other groups (b-c).

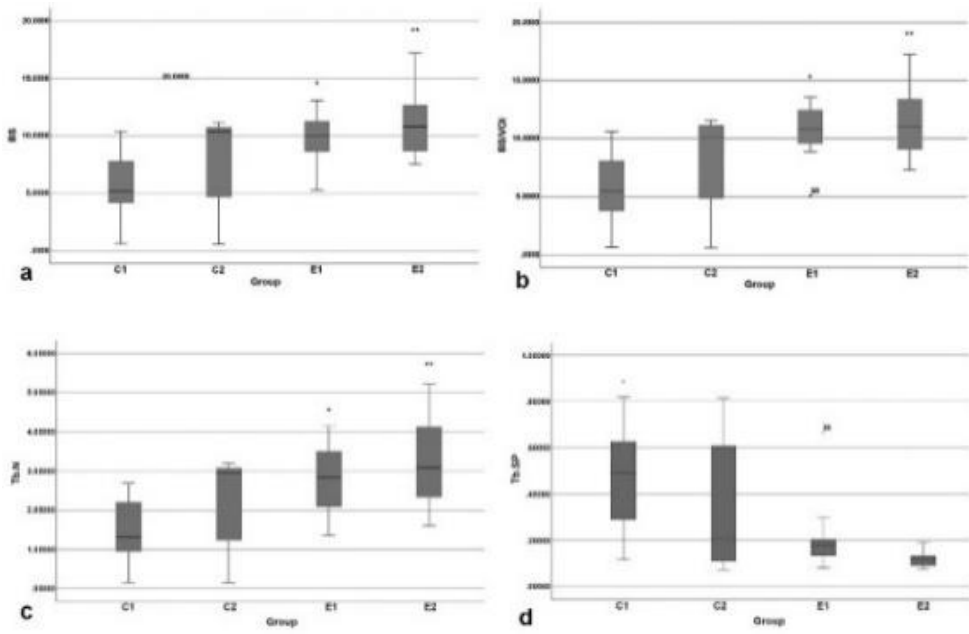

Figure 9. Comparison of micro-CT parameters between the groups. BS (a), bone surface and BS/VOI (b), Tb.N (C), Tb.Sp (d) (*, **$p< 0.05$).

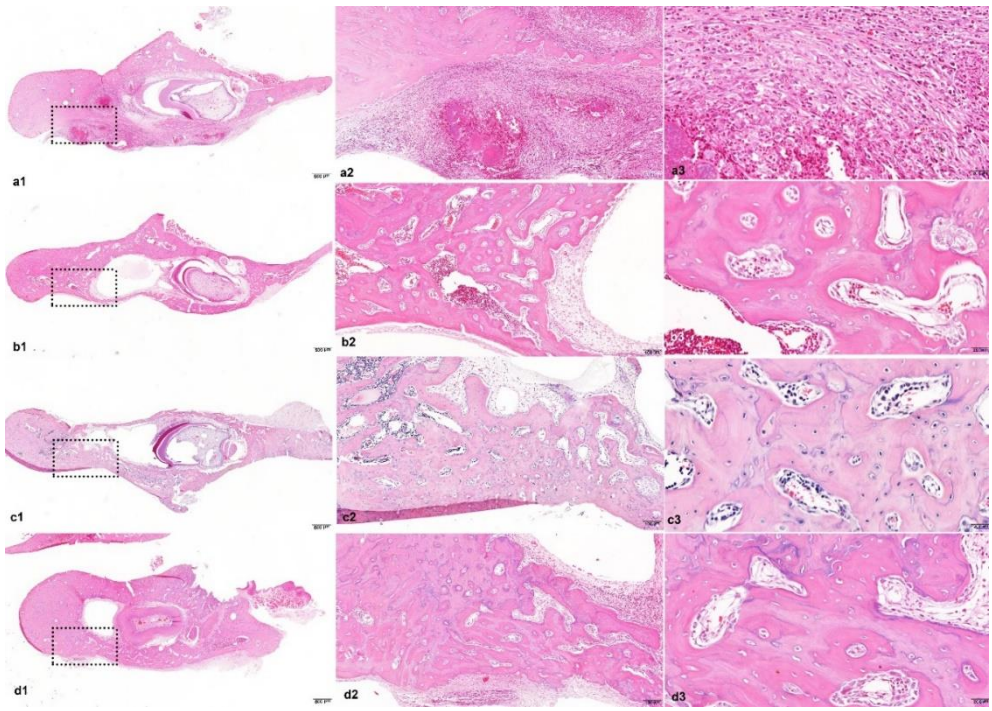

Figure 10. Representative histological images of the specimens following 4 weeks of treatment stained with H&E. In the C1 group, intense inflammatory infiltration is observed, 2x (a1). Magnification of the rectangles, 10x, 40x (a2-a3). The C2 group showed bone healing with osteoblastic cell lining in the parenchymal tissue found at the center of the defect area with evidence of inflammatory infiltrates (b1). Magnifications of the rectangles at 10x, 40x (b2-b3). The E1 group showed loose marrow fibrosis and scattered lymphocytic inflammatory infiltrates, 2x (c1). High power view of the rectangles, 10x, 40x (c2-c3). The E2 group showed increased osteophytic bone formation, 2x (d1). High power view of the rectangles at 10x, 40x (d2-d3).

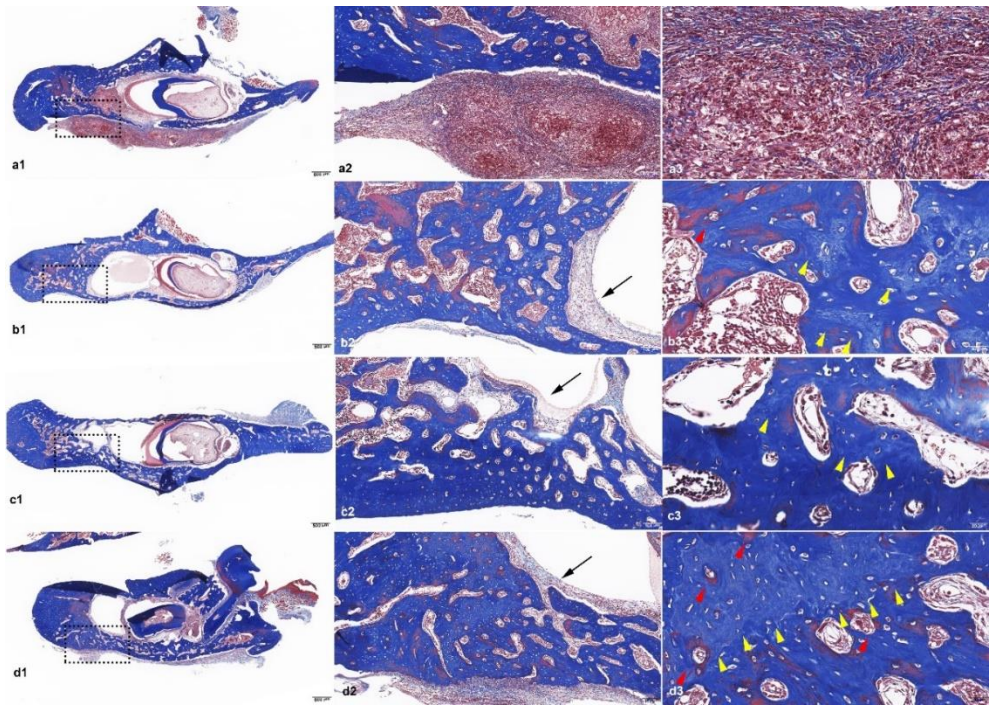

Figure 11. Representative histological images following 4 weeks of treatment stained with MT. The C1 group were stained with thick blue color, indicating old bone, while no new bone formation stained with bright blue color were observed (a1). Magnification of the rectangles, 10x, 40x (a2-a3). MT stain for bone regeneration in the C2 group at 2x (b1). Magnification of the rectangles, 10x, 40x (b2-b3). The MT stain of E1 group showed new bone formation stained with bright blue color and new blood vessels were observed, 2x (c1). Magnification of the rectangles, 10x, 40x (c2-bc3). The E2 group showed active bone remodeling with the thickest compact new bone formation in the defect area compared to that of other groups, 2x (d1). An increased number of Haversian canals with osteoblast rimming and new blood vessel formation stained with thick red color by the MT stain were observed at 10x, 40x magnification (d2-d3). Black arrow, parenchymal tissue, Yellow arrowhead, new bone formation, Red arrow, blood vessel formation.

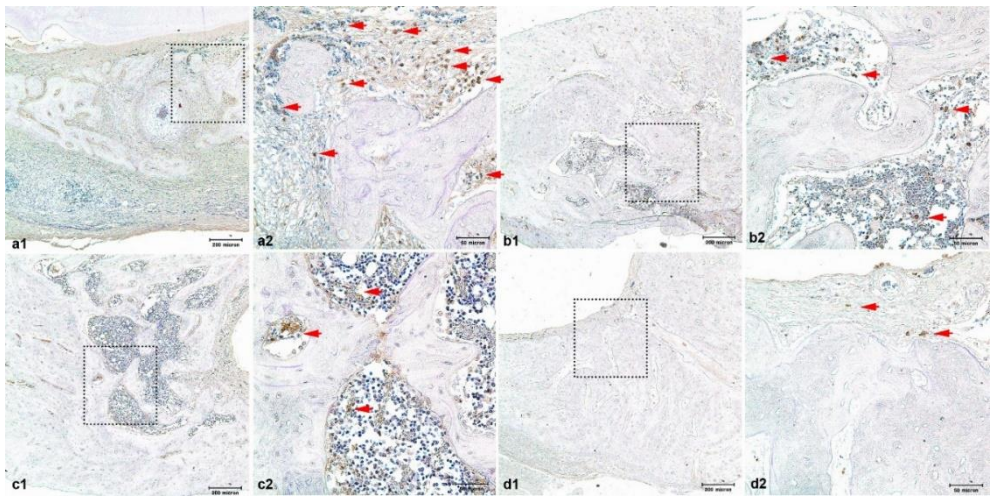

Figure 12. IL-6 antibody staining in the C1 group (a), C2 group (b), E1 group (c), and E2 group (d). a1 IL-6 antibody staining with original magnification 10x, a2, magnified view of the selected area from a1, 40x. The red arrowheads mark the stained antibodies in the defect area.

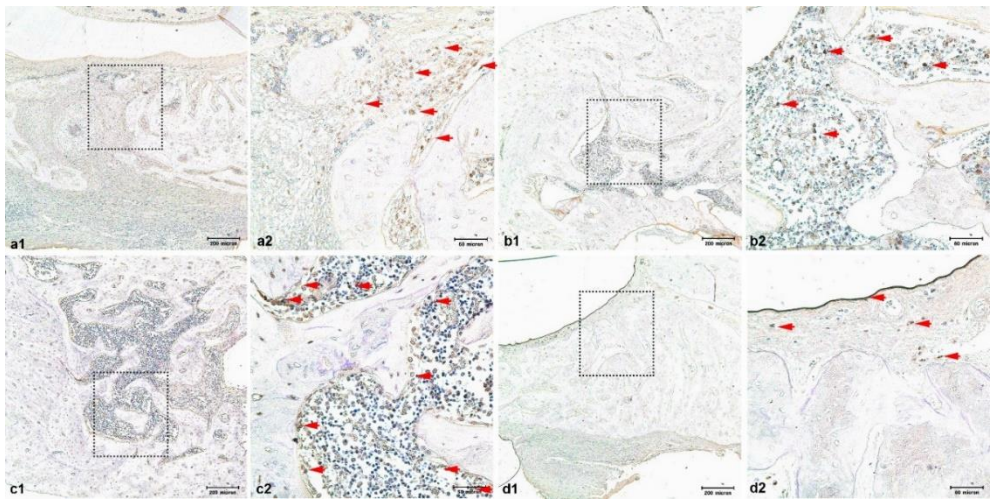

Figure 13. TNF-α antibody staining in the C1 group (a), C2 group (b), E1 group (c), and E2 group (d). a1, TNF-α antibody staining with original magnification 10x, a2, magnified view of the selected area from a1, 40x. The red arrowheads mark the stained antibodies in the defect area.

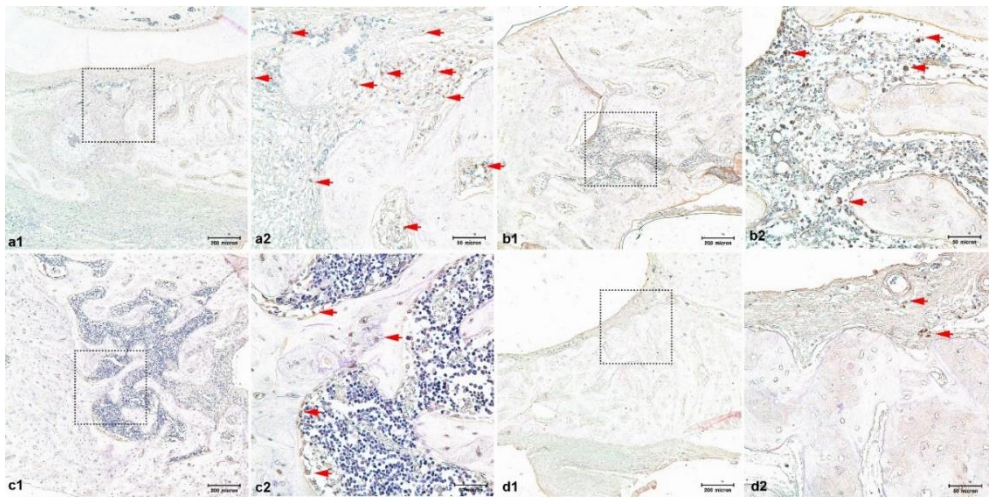

Figure 14. VEGF-A antibody staining in the C1 group (a), C2 group (b), E1 group (c), and E2 group (d). a1 VEGF-A antibody staining with original magnification 10x, a2, magnified view of the selected area from a1, 40x. The red arrowheads mark the stained antibodies in the defect area.

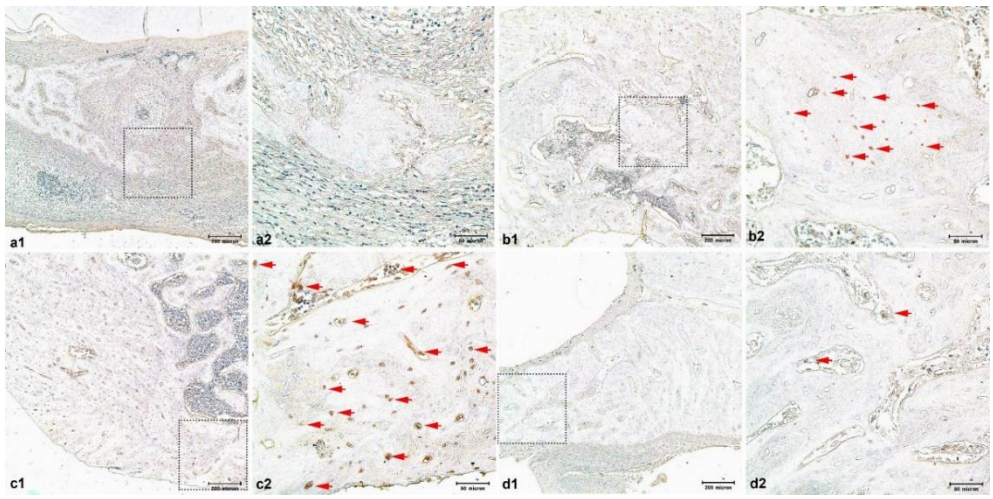

Figure 15. TNF-b1 antibody staining in the C1 group (a), C2 group (b), E1 group (c), and E2 group (d). a1 TNF-b1 antibody staining with original magnification 10x, a2, magnified view of the selected area from a1, 40x. The red arrowheads mark the stained antibodies in the defect area.

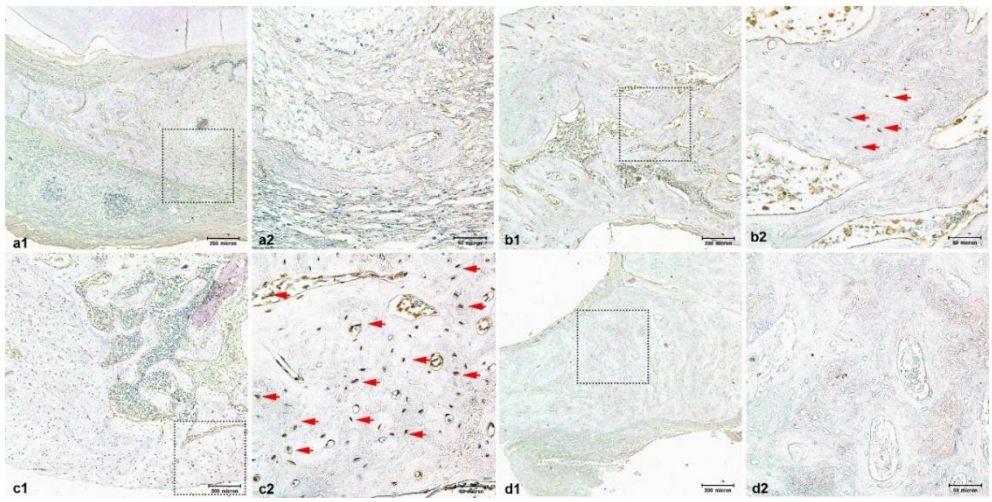

Figure 16. ALP antibody staining in the C1 group (a), C2 group (b), E1 group (c), E2 group (d). a1 ALP antibody staining with original magnification 10x, a2, magnified view of the selected area from a1, 40x. The red arrowheads mark the stained antibodies in the defect area.

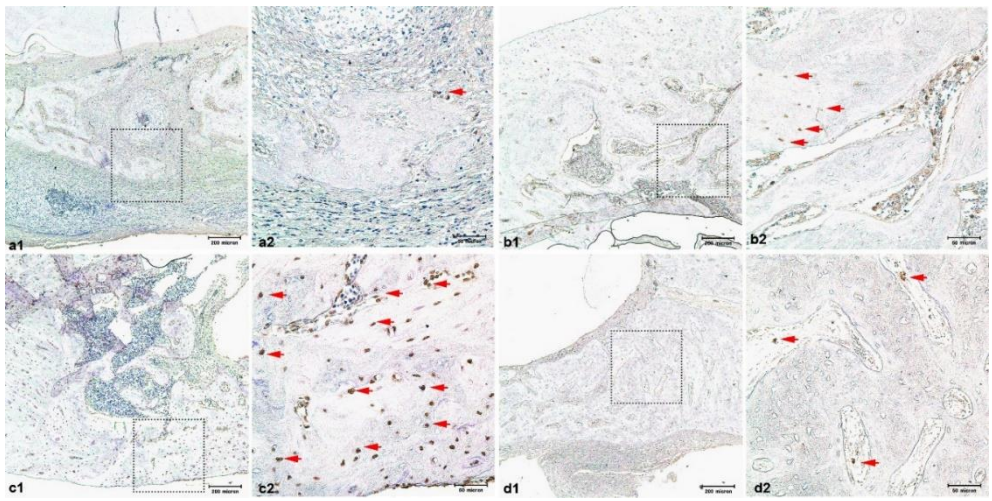

Figure 17. OPN antibody staining in the C1 group (a), C2 group (b), E1 group (c), and E2 group (d). a1 OPN antibody staining with original magnification 10x, a2, magnified view of the selected area from a1, 40x. The red arrowheads mark the stained antibodies in the defect area

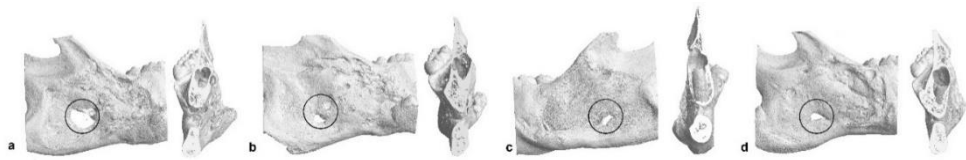

Figure 18. 3D reconstructed images of the C1 (a), C2 (b), E1 (c), and E2 (d) groups. Images show the enhanced bone healing in the round defect in the E1 and E2 groups.

-국문 초록-

백서 하악 골수염에서 감압술 효과

Buyanbileg Sodnom-Ish
서울대학교 대학원 치의과학과 구강악안면외과전공
(지도교수 김 성 민)

연구의 배경 및 목적

턱의 골수염 (Osteomyelitis, OM) 은 대개 만성적인 치성 감염이나 턱뼈를 파괴하는 여러 가지 다른 이유로 인해 발생한다. 포도상구균(*Staphylococcus aureus, S. aureus*) 과 같은 미생물은 중요한 병원균이다. 악안면 낭포종에 드레인을 이용한 감압술은 신뢰할 수 있는 치료방법으로 낭포종 내벽에 배농을 위한 최소한의 배관을 뚫어 낭포종의 크기의 줄이고, 낭포종의 내압을 줄임으로써 주변으로부터 점진적인 뼈 성장을 가능하게 한다. 이 연구의 목적은 하악 골수염 백서 동물 모델에서 감압술의 효과에 대해서 알아보는 것이다.

연구방법

평균 몸무게 230.13±13.87 의 8 주 된 수컷 Sprague-Dawley 백서 14 마리를 실험에 사용하였다. 하악에 직경 4 mm 의 결손부를 만들어 $1x10^7$

CFU/ml 농도의 포도상구균 20ul 를 결손부에 주입하여 골수염을 유발하였다. 백서는 치료방법에 따라 대조군은 치료하지 않은 그룹을 대조군 1 (control, C1), 소파술을 시행한 그룹을 대조군 2 (control, C2) 로 설정하였고, 실험군은 소파술, 드레인을 이용한 감압술을 시행한 그룹을 실험군 1 (experimental 1, E1), 소파술, 드레인을 이용한 감압술과 드레인을 통해 생리식염수로 세척을 시행한 그룹을 실험군 2 (experimental 2, E2) 로 설정하였다. 치료 후 4 주에 백서를 희생하여 마이크로 단층촬영 (micro-CT), 헤마톡실린-에오신 (hematoxylin and eosin, H&E) 과 Masson's trichrome 염색을 사용한 조직학적 분석을 시행하였고, 염증 관련 항체 IL-6 와 TNF-α, 신생 혈관 관련 항체 VEGF-A 와 TGF-β1, 골 형성 관련 항체 OPN 와 ALP 항체를 사용해 면역화학적 분석을 시행하였다.

연구결과

백서 하악골 골수염 모델에서 포도상구균에 의해 골수염이 유발된 것을 임상과 실험적 결과로 확인하였다. 마이크로 단층촬영 (micro-CT) 에서 골 치유에 대한 대부분의 매개변수는 대조군 1 (C1) 과 대조군 2 (C2) 그룹에서 현저히 낮았다. 특히 실험군 2 (E2) 에서 대조군 1 (C1) 과 대조군 2 (C2) 에서 볼 수 있는 것 보다 골량 (bone volume) 과 골밀도 (bone mineral density, BMD) 가 크게 향상되었고, bone volume/volume of interest 가 유의미하게 높았다 ($p < 0.05$). 조직학적 분석에서 실험군 1 (E1) 과 실험군 2 (E2) 에서 결손부위에 발견되는 골세포 (osteocyte) 의 수가 현저히 많은 것으로 두드러진 골 치유를 보였다 ($p < 0.05$). 면역화학적 염색에서 실험군 2 (E2) 는 대조군 1 (C1) 에 비해 IL-6 의 표현이 가장 약했고, TNF-α 의 표현은 다른 그룹과 비교하여 실험군 1 (E1) 에서 강하게 착색되었다. VEGF-A 의 표현은 실험군 2 (E2) 에 비해 대조군 1 (C1) 에서 가장 높았고, TGF-β1, ALP, OPN 표현은 실험군 1 (E1) 에서 현저하게 높았으며, 대조군 1 (C1) 에서는 다른 그룹과 비교했을 때 TGF-β1, ALP, OPN 표현이 없었다.

결론

마이크로 단층촬영 (micro-CT), 헤마톡실린-에오신 (hematoxylin and eosin, H&E)과 Masson`s trichrome 염색을 사용한 조직학적 분석 및 면역화학적 분석은 골수염 백서 모델에서 드레인을 이용한 감압술이 기존의 수술적 치료에 비해 이상적인 골 치유 결과를 보였음을 확인하였다. 이러한 결과를 바탕으로 임상의는 악안면 골수염 치료를 위해 배농 (drainage) 과 세척 (irrigation) 을 동반한 감압술을 사용하는 것을 권장할 수 있을 것으로 사료된다.

주요어: 턱의 골수염, 포도상구균, 감암술, 배농, 마이크로 단층촬영, 조직학 및 면역화학적 연구
학번: 2019 -29083